

Article

# Experimental Study of Sound Pressure Level in Hydraulic Power Unit with External Gear Pump

Alexander Mitov <sup>1,\*</sup> , Krasimir Nedelchev <sup>2</sup> and Ivan Kralov <sup>2</sup>

<sup>1</sup> Department of Hydroaerodynamics and Hydraulic Machines, Technical University of Sofia, Kliment Ohridski 8 Boulevard, 1000 Sofia, Bulgaria

<sup>2</sup> Department of Mechanics, Technical University of Sofia, Kliment Ohridski 8 Boulevard, 1000 Sofia, Bulgaria; krasined@tu-sofia.bg (K.N.); kralov@tu-sofia.bg (I.K.)

\* Correspondence: a\_mitov@tu-sofia.bg; Tel.: +359-886208937

**Abstract:** The article presents the results of an experimental study of the sound pressure level (*SPL*) caused by a hydraulic power unit with an external gear pump. The study was carried out with a specially developed laboratory experimental setup based on a common architecture used in hydraulic power units. Both the hydraulic system and the measuring equipment used are described in detail. The design of the experimental studies performed, including two main configurations with specific parameters regarding the operating modes of the system, is presented. The experimental results obtained are presented in the form of magnitude frequency responses which are compared in accordance with the experiment design. An analysis of the results obtained is performed using various quantitative indicators. For specific operating modes, parametric models were derived by approximation of the experimental data. The resulting models can serve in future work to reduce the *SPL* by passive or active means (e.g., frequency control of the electric motor). The quantitative analysis can serve as a basis of comparison with results obtained after adding passive (damping ring, etc.) or active means to reduce the *SPL*.

**Keywords:** experimental study; sound pressure level; external gear pump



**Citation:** Mitov, A.; Nedelchev, K.; Kralov, I. Experimental Study of Sound Pressure Level in Hydraulic Power Unit with External Gear Pump. *Processes* **2023**, *11*, 2399. <https://doi.org/10.3390/pr11082399>

Academic Editor: Olympia Roeva

Received: 14 July 2023

Revised: 5 August 2023

Accepted: 7 August 2023

Published: 9 August 2023



**Copyright:** © 2023 by the authors. Licensee MDPI, Basel, Switzerland. This article is an open access article distributed under the terms and conditions of the Creative Commons Attribution (CC BY) license (<https://creativecommons.org/licenses/by/4.0/>).

## 1. Introduction

Hydraulic drive systems are a major source of noise and vibration in various machines. The widespread use of this type of drive system, both for industrial and mobile applications, leads to the need to reduce the noise of hydraulic drives [1]. This task is essential to increase the reliability and competitiveness of these systems, and also to improve operating conditions and protect the environment.

It is impossible to replace hydraulic drives in certain applications requiring a high level of transmitted power with relatively compact dimensions, high control performance, etc. However, considering the increase in the requirements for various mechatronic systems and in the use of clean technologies, the requirements for a relatively low noise level are constantly increasing. For many applications, the sound pressure level (*SPL*) cannot exceed 65 dB(A). In other applications, such as forklifts, the *SPL* cannot exceed 75 dB(A), and for metalworking machines and industrial robots, the permissible level is 70 to 72 dB(A) [2–4]. In all of these cases, these levels are difficult to achieve when using a hydraulic drive. In some of these applications, the *SPL* measured under normal operating conditions reaches 90 dB(A) due to the use of a hydraulic drive system. These circumstances have motivated a number of researchers to develop and implement ways of reducing the *SPL* in hydraulic drive systems [4–7].

Research available to date shows that noise in hydraulic drives is mainly caused by the hydraulic pump, due to the flow rate ripple and pressure pulsations, which are consequences of the design features and limitations of these systems [8–10]. Besides the pump, however, there are other sources of noise in these systems, such as the electric motor,

the coupling, the process of the working fluid flowing through the pipelines, pressure-relief valves, throttles, and other control and auxiliary hydraulic devices that are features of every hydraulic drive system.

Focusing on the pump, the flow rate ripple is highest for external gear pumps. In older designs, the ripple can reach a level of about 20% compared to other types of displacement rotary pumps, such as the axial piston pump [11]. This is why the noise level of external gear pumps is the highest, which has motivated a number of studies aimed at finding measures to reduce it. These studies can be conditionally divided into two main groups. The first group focuses on research and development dedicated to structural changes in external gear pumps [12–14], and the second group focuses on changes in the manner of installation in hydraulic power units to reduce the noise of the system as a whole [6,15]. It is relevant to note that there are standards [2,3] and standard testing procedures [16,17] for clearly determining the *SPL* caused by external gear pumps. However, they typically require that this measurement be carried out either in an anechoic chamber [18,19] or by measuring sound intensity. In both cases, the pump is mounted outside the tank, and this configuration is found in most research on the subject. However, from a practical point of view, in most cases this type of pump is installed inside the tank of the hydraulic power unit, and therefore the *SPL* remains relatively high and does not meet the requirements. This problem has motivated the authors to experimentally investigate the *SPL* caused by an external gear pump used in a common configuration of a hydraulic power unit under normal operating conditions.

The main goal of the article is to present experimental results and analysis of the *SPL* caused by an external gear pump installed inside the tank of a hydraulic power unit. In contrast to other similar studies [6,15,16], the experimental determination of the *SPL* was carried out under the normal operating conditions in which hydraulic drives for various industrial applications most often operate. Our laboratory experimental setup was designed and realized toward this end. The pump experimental tests were performed at different rotation frequencies and different values of output pressure load. The obtained results are presented in the form of magnitude frequency responses. The analysis was performed on the basis of various quantitative indicators: A-weighted *SPL*, average A-weighted *SPL*, maximum *SPL*, minimum *SPL* and area of the magnitude frequency response (calculated by Riemann's integral formula). For specific operating modes, parametric models were derived by approximation of the experimental data to obtain transfer functions of the *SPL* magnitude frequency responses. The resulting models can serve in future work to reduce the *SPL* by passive or active means (e.g., frequency control of the electric motor). The quantitative analysis can serve as a basis of comparison with results obtained after adding passive (damping ring, etc.) or active means to reduce the *SPL*.

The article is organized as follows: Section 2 shows the detailed description of the experimental system and measuring equipment; Section 3 presents the design of the experiment; Section 4 depicts the experimental results; Section 5 shows the analyses of the experimental results; parametric models of the *SPL* are derived in Section 6; and in Section 7 some conclusions are given.

## 2. Experimental System Description

We designed and realized a laboratory setup for the experimental study of *SPL* caused by an external gear pump installed in a hydraulic power unit. The purpose of the experimental system is to match the architecture of commonly used power units in hydraulic drives for different applications. Most often, hydraulic power units are designed and implemented according to the specific requirements of their application, but regardless of this, they contain basic components such as a pump, an electric motor to drive the pump mounted on the cover with a standard mounting flange, a coupling, a discharge line, a pressure-relief valve, and other control and regulating throttling devices. Not infrequently, these components are sources of noise and vibration in the system as a whole. The use of an external gear pump leads to an increase in noise regardless of the fact that it is most

often located inside the tank and is immersed in the working fluid. This motivated the design and realization of a hydraulic power unit with such a pump. The hydraulic circuit diagram of the developed experimental setup is presented in Figure 1.

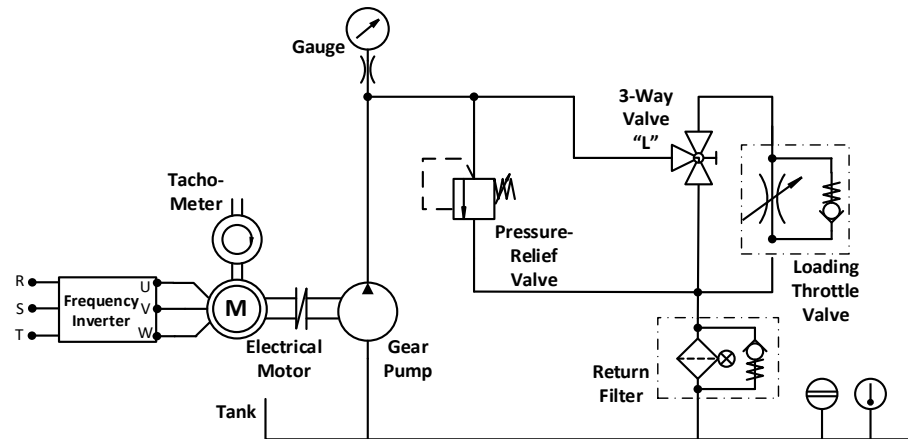


**Figure 1.** Hydraulic circuit diagram of the experimental system.

The hydraulic system consists of a tank with a volume of 120 L and an external gear pump with a displacement volume of  $19 \text{ cm}^3$  driven by a 7.5 kW three-phase asynchronous electric motor with a nominal rotation frequency of  $1500 \text{ min}^{-1}$ . A direct operated pressure-relief valve and a variable throttle valve with an integrated check valve are connected in parallel in the discharge pipeline of the pump. The outlet of the throttle valve is connected to a return filter group. A three-way, two-position L-type ball valve is connected in parallel between the pressure-relief valve and the throttle valve to switch between the loading mode and the non-loading mode of the system. In the non-loading mode, the pump discharge line is connected directly to the tank.

The experimental setup needs to enable the pump to be tested in different operating modes defined by different rotation frequencies and different output pressure loads. For this purpose, a modern frequency inverter is used in the system, enabling the rotation frequency of the electric motor to be changed precisely within the range of 0 to  $1500 \text{ min}^{-1}$ . The rotation frequency is measured directly from the electric motor by means of a laser digital tachometer. In this aspect, a short shaft with a suitable mark is threaded into the main shaft on the side of the cooling fan of the electric motor to measure the rotation frequency. The pressure-relief valve sets the maximum pressure value in the system, and the throttle valve changes the output pressure load from the minimum to the maximum value. The pressure measuring is performed with a gauge with accuracy class 0.6 connected through a pressure measuring connector in the pressure-relief valve body.

The main components and the parameters used for the implementation of the experimental setup are listed in Table 1. Before building the system, a 3D model (Figure 2) was developed to define the preliminary composition of the hydraulic power unit.

As can be seen from the 3D model, the pump is installed inside the tank. The coupling between it and the electric motor consists of a standard mounting flange and a clutch with an elastic element. The connection between the mounting flange and the tank cover is direct through bolts, without an additional damping ring. The pump discharge pipeline exits the tank through a bite-type bulkhead coupling fitting. The rest of the piping and the hydraulic control and regulating equipment are located on the cover, without additional mounting brackets. The diameter of the pipelines is  $15 \times 1.5 \text{ mm}$ , and bite-type fittings are used. The body of the pressure-relief valve and the tap serve as tees in the system, as is common practice. The purpose of the preliminary composition is maximum compliance with the hydraulic circuit diagram (Figure 1) and the subsequent implementation.

**Table 1.** Experimental system components.

No.	Component	Model	Parameters
1	Tank	Custom construction	$V = 120 \text{ L}$
2	Electric motor	Miksan 134 M4	$P_{EM} = 7.5 \text{ kW}$ $n = 1500 \text{ min}^{-1}$
3	External gear pump	20A(C)19X006	$V_p = 19 \text{ cm}^3$
4	Direct-operated pressure-relief valve	CPL40/12	$q_{\max} = 40 \text{ L/min}$ $\Delta p_{\max} = 25 \text{ MPa}$
5	Throttle check valve	VRFU9003	$q_{\max} = 50 \text{ L/min}$ $\Delta p_{\max} = 35 \text{ MPa}$
6	3-Way ball valve, L-type	GB3VH	$q_{\max} = 50 \text{ L/min}$ $\Delta p_{\max} = 35 \text{ MPa}$
7	Return filter group	MPF1002AG3P25NBP01	$q_{\max} = 50 \text{ L/min}$ $\eta = 25 \mu\text{m}$
8	Frequency inverter	HNC HV 100	$U = 380 \text{ V}$ $P = 7.5 \text{ kW}$
9	Sound and vibration measuring device	SVAN 958A SN: 92,313	Digital 4-Channel $f = 0.5 \text{ Hz to } 20 \text{ kHz}$
10	Microphone	MK255 SN: 17,262	$\frac{1}{2}$ $50 \text{ mV/Pa}$
11	Preamplifier	SV12L SN: 95,175	Detachable (TNC)
12	Fold-out tripod	Leica TRI 100	Removable head plate
13	Digital tachometer (laser)	DT2234A	$n_{\max} = 100,000 \text{ min}^{-1}$
14	Accelerometer	TDL 356A16 SN: 265,696	$100 \text{ mV/g}$ $0.5 \text{ to } 5 \text{ kHz}$
15	Acoustic camera (microphone array)	Bionic M 112 SN: 200816HM0112	$33 \text{ to } 120 \text{ dB}$ 112 MEMS-microphones, 24 bit, 48 kHz, $f = 10 \text{ Hz to } 24 \text{ kHz}$
16	Acoustic camera controller	IH I2S-112 SN: 201105HAT112	8 to 32 bits/sample 96 kHz at 64-bit
17	Acoustic camera software	SAB Smart Vision ver. 1.2	Beamforming visualization

**Figure 2.** 3D model of the experimental system.

### 3. Experiment Design

The experimental study of the *SPL* caused by an external gear pump included in a hydraulic power unit was carried out using the experimental setup presented in the previous section, which was specially developed for this purpose. This section is devoted to the design (planning) of the experimental tests and their realization. Vibration measurement and analysis will be the subjects of future study.

The preliminary plan for performing the experiment in relation to the location of the measuring equipment is shown in Figure 3. The plan shows the location (sizes in mm) of the microphones with which the *SPL* was measured. An SVAN958A sound level meter was used, which is a class-1 four-channel sound and vibration analyser appropriate for all applications that require excellent simultaneous sound and vibration assessment. Each of the four input channels can be independently configured for sound or vibration detection with different filters and RMS detector time constants, allowing enormous measurement flexibility. The major advantage of the SVAN958A is the capability to perform advanced analysis simultaneously in the level meter mode. In practice, this allows obtaining broadband results such as  $L_{eq}$ , RMS,  $L_{Max}$ ,  $L_{Min}$ ,  $L_{Peak}$  together with four-channel analysis such as FFT or octave-band analysis [20].

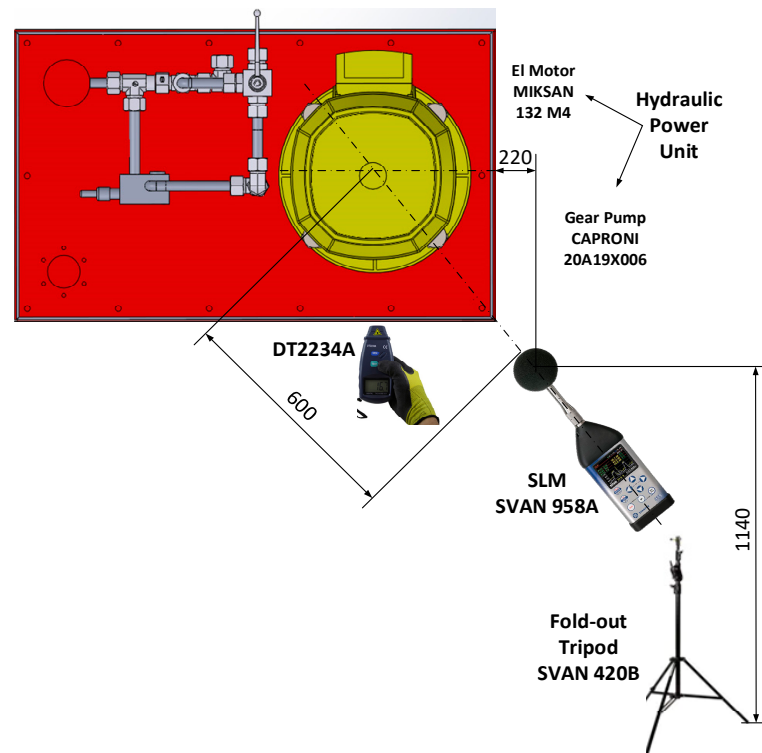


**Figure 3.** Arrangement of measuring equipment.

Following ISO standards for measuring the noise emitted by machinery in various environments (ISO 3740, ISO 3741, ISO 3744, ISO 3745 and ISO 3747) [3,18,19,21,22], first the measurement surfaces and the positions of the microphones were defined. In this case, the choice was determined by the possibility of simultaneous measurement with the SVAN958A and the acoustic camera. The microphones were placed near the area of the main sources of acoustic noise (the electric motor and gear pump). Although sound power is not measured, the sound pressure level is used to assess the effect on the noise emitted by the object under study. Future work will investigate how the microphone placement affects the measurement results.

Regarding the plan of the operating modes in which the experimental measurements were carried out, the typical values of two variable parameters were considered: rotation

frequency  $n_i$  and load pressure  $\Delta p_i$ . The rotation frequency varies in the range of 950 to 1450  $\text{min}^{-1}$  according to the capabilities of the electric motor. The load pressure of the pump in the different operating modes varies in the range of 0 to 15 MPa. The choice of this range stems from the fact that this type of hydraulic pump is operated continuously up to a maximum pressure value of 16 MPa. For short-term operation, it is possible to operate at higher pressures, but not more than 25 MPa. Two configurations of the experimental studies were planned.

In the first configuration, the noise measurements were carried out with the specific values of the output pressure load  $\Delta p_i$  at constant values of the rotation frequency  $n_i$  and at a fixed maximum pressure value  $\Delta p_{PRV}$  set with the pressure-relief valve corresponding to 16 MPa. The different variants of the variable parameters in the first configuration are presented in Table 2. In this case, the load pressure values  $\Delta p_i$  are set by different closing positions of the throttle valve at given fixed pressure-relief valve settings.

Table 2. First configuration of experimental study.

No.	$n_i$	$\Delta p_i$	$\Delta p_{PRV}$	$L_{SPL}(A)$	$L_{SA}(A)$	$L_{oct,max}$	$L_{oct,min}$	$\int_{f_{min}}^{f_{max}} S(f)df$
	$\text{min}^{-1}$	MPa	MPa	dB	dB	dB	dB	Hz
1	950	0	16.00	79.04	54.76	74.70	26.00	897.07
2		5.00		79.90	54.47	75.30	21.30	912.02
3		7.50		80.47	55.23	75.70	21.00	926.30
4		10.00		80.42	55.73	75.80	20.70	934.22
5		12.50		81.85	56.63	78.70	22.40	948.02
6		15.00		81.84	57.14	78.40	21.50	950.70
1	1150	0	16.00	79.66	56.03	74.10	23.50	904.85
2		5.00		78.84	55.87	72.90	23.30	918.99
3		7.50		79.98	56.46	75.80	23.90	938.32
4		10.00		80.30	57.41	75.00	24.10	944.20
5		12.50		80.73	59.00	74.50	25.50	951.93
6		15.00		80.89	57.61	74.30	23.40	952.90
1	1250	0	16.00	77.05	53.43	70.20	24.60	891.69
2		5.00		76.14	52.90	70.20	24.40	907.95
3		7.50		77.89	54.46	71.20	25.40	925.37
4		10.00		78.91	55.48	73.20	24.60	937.20
5		12.50		79.82	56.85	73.10	24.60	944.56
6		15.00		81.96	57.36	76.40	24.50	950.29
1	1350	0	16.00	76.08	53.70	69.60	24.90	896.19
2		5.00		81.17	55.78	75.50	25.50	924.72
3		7.50		82.58	57.90	76.30	26.40	943.06
4		10.00		84.28	59.35	78.70	26.70	958.00
5		12.50		84.38	59.76	78.30	26.20	967.82
6		15.00		85.14	59.98	79.10	25.90	975.17
1	1450	0	16.00	81.37	55.84	77.60	26.20	924.00
2		5.00		79.91	56.84	71.80	26.20	936.66
3		7.50		81.64	59.04	73.10	28.20	972.54
4		10.00		82.94	60.36	76.60	27.70	1005.20
5		12.50		85.59	62.01	80.40	27.80	1048.90
6		15.00		86.74	62.96	82.20	27.60	1063.50

Experiment design

In the second configuration, the SPL measurements were performed at a load pressure  $\Delta p_i$  equal to the pressure-relief valve setting  $\Delta p_{PRV}$ , which is used in the relief modes of the valve. The variants of modes in the second configuration are shown in Table 3. In

these modes, the pump flow rate flows through the pressure-relief valve. The second configuration modes are realized with a fully closed loading throttle valve. The motivation for measuring noise in the second configuration stems from the fact that in hydraulic systems with throttle control of the speed of the hydraulic cylinders or motors, the main pressure-relief valve is in the relief mode, and in this way part of the pump flow is released into the tank as a result of throttling. In this mode, the valve introduces additional noise due to the small opening sections and high flow velocities. In systems with this type of regulation, typically a fixed-displacement pump is used, which is often an external gear pump. The different variants of variable parameters in the second configuration are presented in Table 3.

**Table 3.** Second configuration of experimental study.

No.	$n_i$	$\Delta p_i$	$\Delta p_{PRV}$	$L_{SPL}(A)$	$L_{SA}(A)$	$L_{oct,max}$	$L_{oct,min}$	$\int_{f_{min}}^{f_{max}} S(f)df$
	$min^{-1}$	MPa	MPa	dB	dB	dB	dB	Hz
1	950	16.00	16.00	83.22	59.06	76.60	23.20	973.50
2		10.00	10.00	82.77	58.75	78.80	32.20	949.23
3		7.50	7.50	81.26	57.44	73.70	20.60	957.39
4		5.00	5.00	82.26	55.80	79.00	20.20	910.43
1	1150	16.00	16.00	83.09	59.85	76.80	25.60	985.66
2		10.00	10.00	81.94	60.73	73.40	30.40	991.29
3		7.50	7.50	82.34	59.08	76.20	23.90	971.75
4		5.00	5.00	80.59	57.37	74.60	23.40	928.78
1	1250	16.00	16.00	84.80	59.05	78.90	25.50	993.24
2		10.00	10.00	81.41	57.94	75.10	25.60	992.52
3		7.50	7.50	82.83	57.91	77.40	24.10	979.12
4		5.00	5.00	79.47	56.19	72.90	29.00	928.08
1	1350	16.00	16.00	85.06	60.40	78.20	29.80	1003.20
2		10.00	10.00	82.62	59.53	76.20	25.20	979.99
3		7.50	7.50	84.76	60.35	80.20	24.90	975.72
4		5.00	5.00	81.92	57.68	77.90	30.60	929.82
1	1450	16.00	16.00	86.53	61.25	83.00	28.70	1031.30
2		10.00	10.00	85.23	61.58	78.70	27.50	1052.60
3		7.50	7.50	86.57	62.20	82.40	26.20	1060.90
4		5.00	5.00	83.24	60.65	75.90	30.50	1019.90

min Results analysis max

Tables 2 and 3 describe the variability of the operating modes of the experimental study and quantitative indicators for analysis (discussion) of the results.

The realization of the laboratory experimental system, in accordance with the preliminary design in the form of a 3D model and the subsequent design of the experimental studies, is shown in Figure 4. For confirmation of the main sources of sound and additional analysis of the obtained experimental results, a Bionic M 112 acoustic camera was used. It has a microphone array with a diameter of 1 m, consisting of 112 microphones, and is engineered for use from 250 Hz using the beamforming method. The optimized microphone distribution guarantees a perfect sound source localization and a high dynamic range [23]. The acoustic camera is shown in Figure 5.



Figure 4. Implementation of experimental system.



Figure 5. Acoustic camera.

#### 4. Experimental Results

At the beginning of the experiment, the background noise was measured. The difference between the background noise and the noise generated during the operation of the hydraulic power unit is more than 20 dB per 1/3 octave for the studied frequency range (from 100 Hz to 20,000 Hz). The results shown do not exclude background noise. The background noise measurement is only used to check whether the measurement results are affected. The results show that the measurement results were not affected, so no correction of the measured values was necessary. A correction is required if the difference between the background noise and the noise generated during the operation of the object is less than 15 dB (ISO 3744-2013, ISO 3745-2014, ISO 3747-2013, etc.) [3,18,19].

The obtained results for the two configurations of the experimental studies are presented in the form of logarithmic magnitude frequency responses showing the change of the *SPL* in 1/3-octave frequency bands. The initial data processing to obtain separate data sets for each of the modes was performed using SvanPC++<sup>®</sup> (ver. 3.4.9) software, after which the sets in 1/3-octave frequency band data format were imported in MATLAB<sup>®</sup> (ver. R2009b).

Results are presented for only the portion of the study corresponding to typical operating modes for this type of pump [24].

The next three figures show the results of the *SPL* from the first configuration (Table 2) for different rotation frequencies  $n_i$  corresponding to the minimum, average and maximum according to the capabilities of the experimental system. Figure 6 refers to  $950 \text{ min}^{-1}$  rotation frequency of the electric motor, showing the *SPL* under different pressure load modes in the interval 0 to 15 MPa. Figures 7 and 8 show the analogous results corresponding to  $1250 \text{ min}^{-1}$  and  $1450 \text{ min}^{-1}$ .

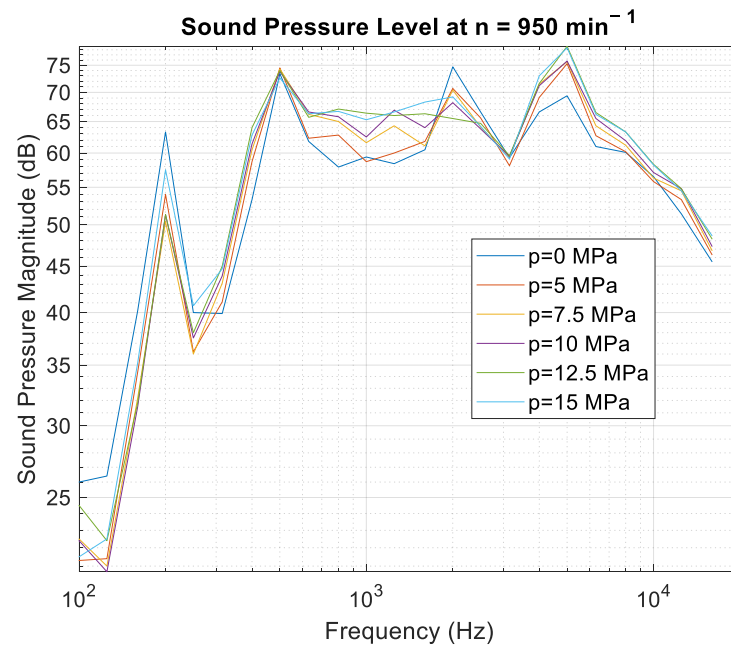


Figure 6. Experimental *SPL* magnitudes at  $n = 950 \text{ min}^{-1}$ .

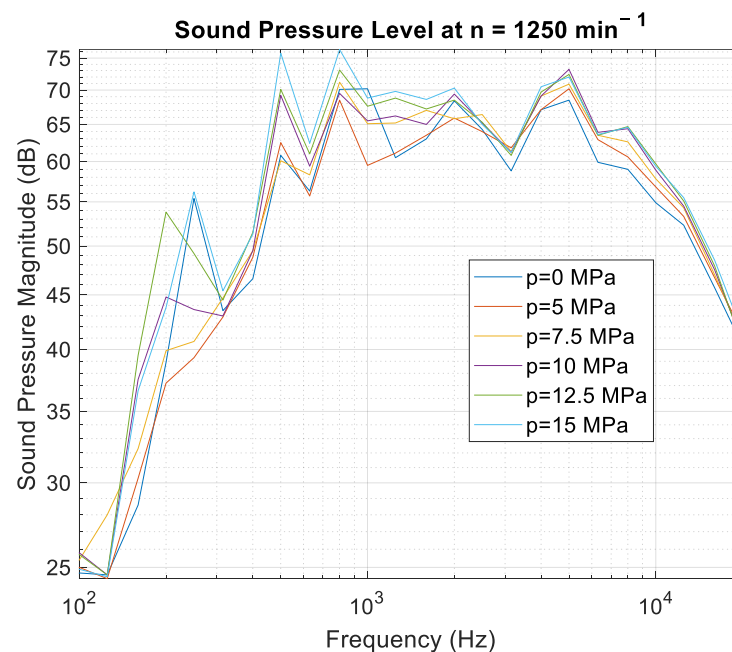
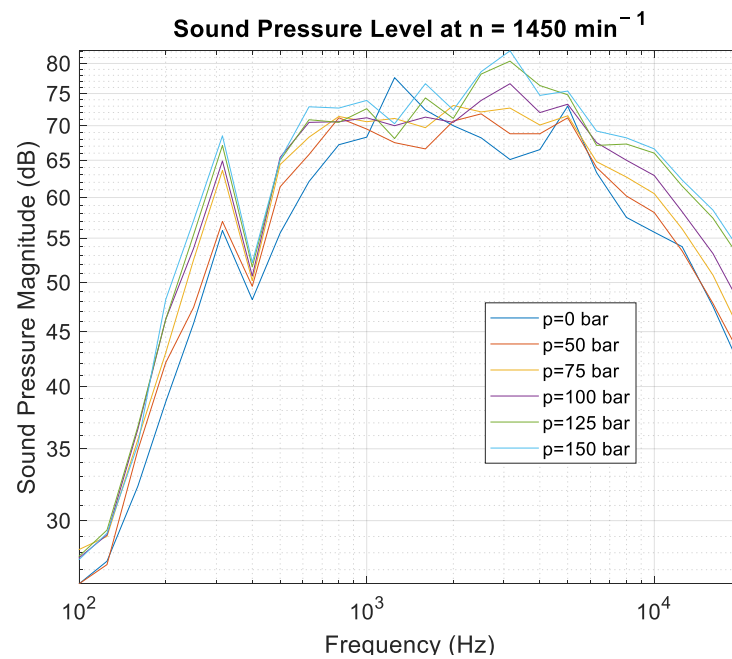
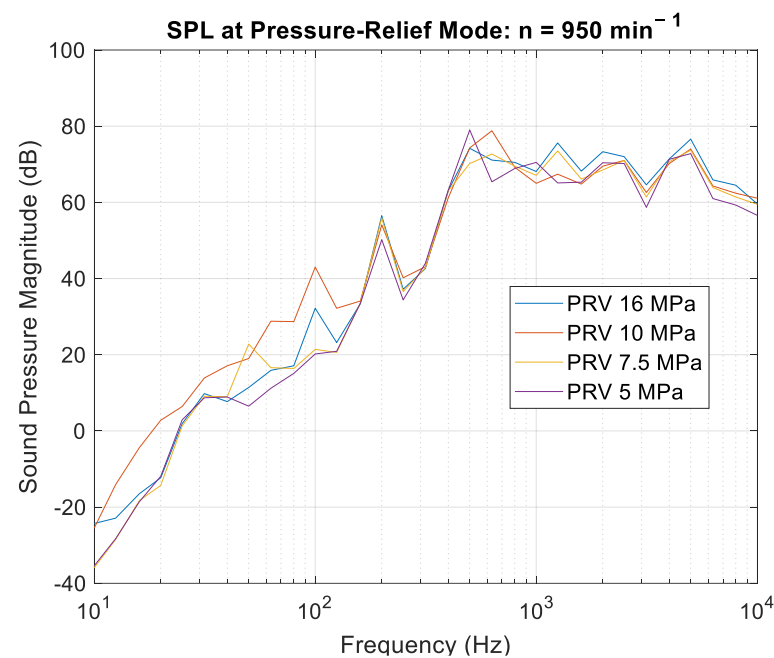


Figure 7. Experimental *SPL* magnitudes at  $n = 1250 \text{ min}^{-1}$ .

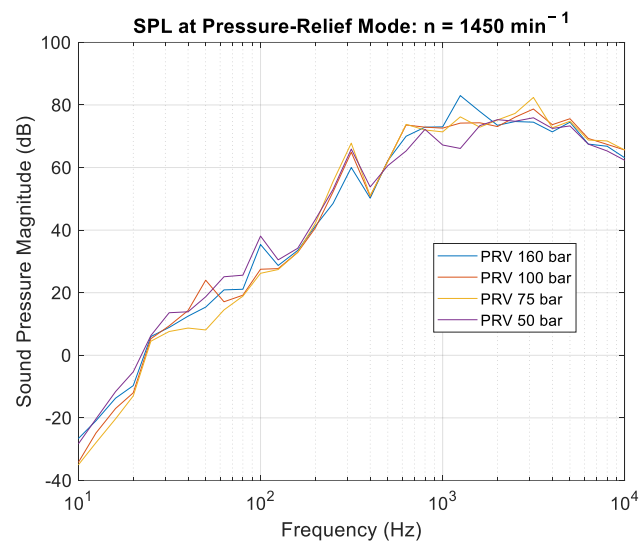


**Figure 8.** Experimental *SPL* magnitudes at  $n = 1450 \text{ min}^{-1}$ .

The results of the second configuration (Table 3) are depicted in Figures 9 and 10. They show the change in *SPL* when the load pressure  $\Delta p_i$  is equal to the pressure  $\Delta p_{PRV}$  setting of the pressure-relief valve, that is, when the valve is in the relief mode. This mode is abbreviated as PRV. These results are again compared for two typical rotation frequencies  $n_i$ , between a minimum of  $950 \text{ min}^{-1}$  and a maximum of  $1450 \text{ min}^{-1}$ .

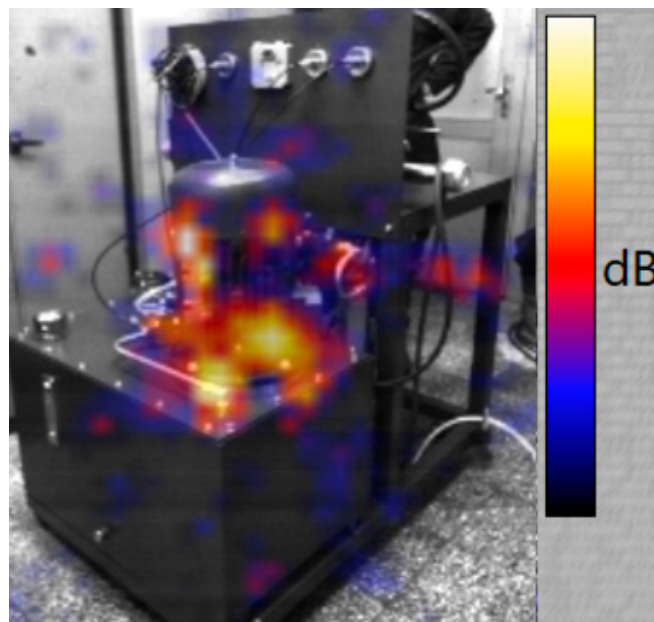


**Figure 9.** Experimental *SPL* magnitudes at PRV mode— $n = 950 \text{ min}^{-1}$ .



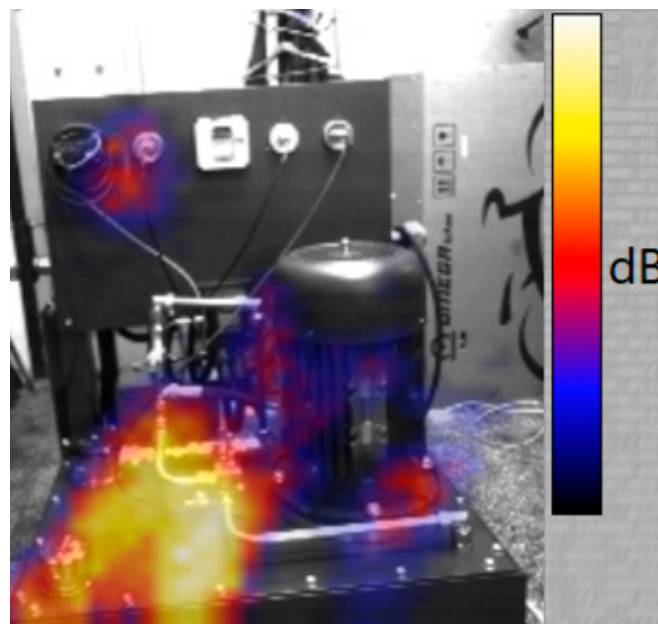
**Figure 10.** Experimental *SPL* magnitudes at PRV mode— $n = 1450 \text{ min}^{-1}$ .

Figure 11 shows the results obtained by recording the *SPL* with the acoustic camera in the non-loading mode of the pump (loading throttle valve fully open) at a nominal rotation frequency of  $1450 \text{ min}^{-1}$ . The recording was made using SAB Smart Vision® (ver. 1.2) software, suitable for this type of acoustic camera, which makes it possible to record a video of sound source localization by beamforming visualization and setting a frequency range during the recording procedure. As can be seen from Figure 11, the main source of sound is the motor-pump group, where the beamforming visualization is focused, and the color corresponds to the upper limit.



**Figure 11.** Experimental results with acoustic camera in non-loading mode.

Figure 12 shows the results obtained by recording the *SPL* with the acoustic camera in the full loading mode of the pump. In this mode, the loading throttle valve is fully closed and the nominal rotation frequency is equal to  $1450 \text{ min}^{-1}$ . Unlike the previous mode, the main source of sound in this mode is the pressure-relief valve, which is in the relief mode. In both cases, the sound camera is located at a 1 m distance from the hydraulic power unit.



**Figure 12.** Experimental results with acoustic camera in full loading mode.

## 5. Discussion of Experimental Results

The analysis of the experimentally obtained results was carried out according to several quantitative indicators [25]: A-weighted  $SPL L_{SPL}(A)$ , average A-weighted  $SPL L_{SA}(A)$ , maximum  $SPL L_{oct,max}$ , minimum  $SPL L_{oct,min}$ , and area of the magnitude frequency response (calculated by Riemann's integral formula). The determination of the listed indicators was carried out on the experimental magnitude frequency responses presented in the previous section for the two configurations. The indicators are calculated for 1/3-octave bands in the interval from 100 Hz to 20 kHz.

The A-frequency weighted  $SPL$  is expressed by

$$L_{SPL}(A) = 10 \log_{10} \sum_{i=1}^n \left( 10^{0.1L_i(A)} \right), \quad (1)$$

where  $n = 24$  is the number of 1/3-octave band frequencies  $f = 100 \dots 20000$  Hz and  $L_i(A)$  is the magnitude of  $SPL$ .

The average value of the A-frequency weighted  $SPL$  is

$$L_{SA}(A) = \sum_{i=1}^{24} \frac{L_i(A)}{n}. \quad (2)$$

The maximum  $SPL$

$$L_{oct,max} = \max_i L_i(A) \quad (3)$$

and minimum  $SPL$

$$L_{oct,min} = \min_i L_i(A). \quad (4)$$

are determined from the experimental data sets.

Determining the area of the frequency response makes it possible to perform not only a qualitative but also a quantitative assessment. Similar to the integral criteria for evaluating the control performance based on transitional processes, this approach is appropriate because results that are similar in nature are evaluated. This enables a more precise analysis of the results. For this purpose, a classical *Riemann* formula [26] is used, defined as follows.

The SPL  $S : [f_{\min}, f_{\max}] \rightarrow \mathbb{R}^+$  is a function defined for positive real numbers  $\mathbb{R}^+$  in the closed frequency interval  $[f_{\min}, f_{\max}]$ , such that

$$f_{\min} = f_0 < f_1 < f_2 \dots < f_n = f_{\max}. \quad (5)$$

The Riemann sum  $J$  of SPL  $S$  over  $[f_{\min}, f_{\max}]$  is determined as

$$J = \sum_{i=1}^n S(f_i^*) \Delta f_i, \quad (6)$$

where  $\Delta f_i = f_i - f_{i-1}$  and  $f_i^* \in [f_{i-1}, f_i]$ .

If the  $f_i^* = f_{i-1}$  for all  $i$ , the method is the *left rule* and gives a *left Riemann sum*. In our case, it is more appropriate to choose the *left rule*.

The closed frequency interval  $[f_{\min}, f_{\max}]$  is therefore divided into  $n$  subintervals, each of length

$$\Delta f = \frac{f_{\max} - f_{\min}}{n}. \quad (7)$$

The points in the interval can be expressed by the following sequence:

$$f_{\min}, f_{\min} + \Delta f, f_{\min} + 2\Delta f, \dots, f_{\min} + (n-2)\Delta f, f_{\min} + (n-1)\Delta f, f_{\max}. \quad (8)$$

In this case, the values of the function are approximated at the left endpoints of  $n$  subintervals, forming multiple rectangles with base  $\Delta f$  and height  $S(f_{\min} + i\Delta f)$ . Realizing this for  $i = 0, 1, \dots, n-1$ , and summing the obtained areas can be summarized as:

$$J_{left} = \Delta f [S(f_{\min}) + S(f_{\min} + \Delta f) + S(f_{\min} + 2\Delta f) + \dots + S(f_{\max} - \Delta f)]. \quad (9)$$

The left Riemann sum amounts to an overestimation if  $S$  decreases monotonically in this interval, and an underestimation if it increases monotonically. The error of this equation will be:

$$\left| \int_{f_{\min}}^{f_{\max}} S(f) df - J_{left} \right| \leq \frac{M_1 (f_{\max} - f_{\min})^2}{2n}, \quad (10)$$

where  $M_1$  is the maximum of the absolute value of  $S(f)$  over the frequency range. This limiting value of the Riemann integral, if it exists, is defined as

$$\int_{f_{\min}}^{f_{\max}} S(f) df = \lim_{|\Delta f| \rightarrow 0} \sum_{i=1}^n S(f_{i-1}) \Delta f_i. \quad (11)$$

Since  $S(f)$  is a dimensionless quantity representing the ratio between the acoustic pressure and the hearing pressure threshold, the unit of the integral  $J$  is Hz.

The analysis of the first configuration results (Table 2) (part of which are depicted in Figures 6–8) shows that the SPL  $L_{SPL}(A)$  increases with increasing pressure load  $\Delta p_i$  at all investigated rotation frequencies  $n_i$ . The lowest  $L_{SPL}(A)$  values at a load of 5 to 12.5 MPa are observed at  $1250 \text{ min}^{-1}$ . This shows that these are the most suitable rotation frequencies in relation to the emitted SPL. Only at  $1150 \text{ min}^{-1}$  is a lower value of  $L_{SPL}(A)$  obtained at a load of 15 MPa. These statements are also confirmed by the other determined indicators.

These observations are also valid for the second configuration (part of which is shown in Figures 9 and 10) in PRV mode. The difference lies in the fact that the considered quantitative indicator increases significantly in terms of value and the interval of its change. For example, at rotation frequency  $950 \text{ min}^{-1}$ , the area changes in the range from 910 to 970 Hz, and at  $1450 \text{ min}^{-1}$  area it changes in the range from 924 to 1063 Hz. The reason for this is the additionally induced noise from the pressure-relief valve, which is in relief mode

when the load pressure  $\Delta p_i$  is equal to the pressure  $\Delta p_{PRV}$  setting of the pressure-relief valve. This is further confirmed by the acoustic camera recording depicted in Figure 12.

The analysis of the second configuration results (Table 3) also shows that at all load values  $\Delta p_i$ , the highest  $L_{SPL}(A)$  is at  $1450 \text{ min}^{-1}$ . It can also be noticed that at 1150, 1250, 1350 and  $1450 \text{ min}^{-1}$ , there are two pronounced minima of  $L_{SPL}(A)$  at 5 and 10 MPa. However, at  $950 \text{ min}^{-1}$  one minima is observed at the 7.5 MPa pressure load. The nature of the change in the maximum value of the  $L_{SPL}(A)$  is similar.

At all rotation frequencies  $n_i$ , the average value of  $SPL L_{SA}(A)$  has a minimum value at a minimum pressure load of 5 MPa. The maximum  $L_{SA}(A)$  value is mostly at a maximum load of 16 MPa, with the exception of  $1450 \text{ min}^{-1}$ , where the maximum  $L_{SA}(A)$  value is at a 7.5 MPa load.

The analysis of the maximum value of  $SPL L_{oct,max}$  can be used to select the optimal operating mode of such hydraulic systems (with throttle control of the speed) in terms of minimum emitted  $SPL$ , in some cases at the expense of flow rate. For this analysis, it is sufficient to determine only  $L_{oct,max}$ . The remaining indicators are useful for a more detailed investigation of the causes of noise emission.

### 6. Parametric Models of SPL

Typically, the problem of reducing pump-induced noise in hydraulic drive systems is solved by the use of either active or passive means. Passive means are easier to implement, and mainly consist of various damping devices, such as a damping ring between the bell-housing motor flange and the lid of the tank, an elastic element in the pump mounting coupling to the electric motor or the housing of the electric motor (requires cooling), additional power unit insulation, etc. [27,28]. Active means are more complex [29], as they are related to improving the frequency control of the electric motor in the case of fixed displacement pumps, or improving the control of the displacement volume in the case of different types of variable displacement pumps. In both cases, a parametric model is required that describes the dynamics of the system with sufficient accuracy. This distinguishes the present approach to obtaining an adequate parametric model and its subsequent use for noise reduction from the approaches often applied in recent years, which have used fluid-structural analysis for the purpose of design changes in the pump [8,12–14].

Producing an analytical model is often a difficult task for more complex systems, because a priori information about the construction of the components is often missing and the large number of components leads to an increase in the order of the dynamic components of the model. In these cases, it is most appropriate to produce a parametric model based on experimentally measured data. In the present case, the authors used a method of identification by approximation of the obtained experimental frequency response. The parametric model of the  $SPL$  experimental frequency response with respect to its magnitude can be expressed as:

$$|S(\theta_i)|^2 = \frac{\left| \sum_{k=0}^n b_k e^{jk\theta_i} \right|^2}{\left| \sum_{k=0}^n a_k e^{jk\theta_i} \right|^2}, \tag{12}$$

where  $e^{j\theta_i} = \frac{-j\omega_i - \alpha}{j\omega_i - \alpha}$ ,  $\omega_i = 2\pi f_i$  and  $\alpha = \sqrt{\omega_{\min}\omega_{\max}}$ .

However, the expansions of the sums are:

$$\begin{aligned} \left| \sum_{k=0}^n b_k e^{jk\theta_i} \right|^2 &= \left( \sum_{k=0}^n b_k \cos(k\theta_i) \right)^2 + \left( \sum_{k=0}^n b_k \sin(k\theta_i) \right)^2 = \\ \sum_{l=0}^n \sum_{k=0}^n b_l b_k (\cos(l\theta_i) \cos(k\theta_i) + \sin(l\theta_i) \sin(k\theta_i)) &= \\ \sum_{l=0}^n \sum_{k=0}^n b_l b_k (\cos((l-k)\theta_i)) &= \sum_{k=0}^n c_k \cos(k\theta_i) \end{aligned} \tag{13}$$

and the equation to be solved is:

$$\sum_{k=0}^n (c_k |S(\theta_i)|^2 - m_k) \cos(k\theta_i) = 0 \quad (14)$$

where  $c_k$  and  $m_k$  are functions of  $a_k$  and  $b_k$  (transfer function coefficients) [30]. The MATLAB<sup>®</sup> function *fitmagfrd* [31] solves this equation, leading to a minimum phase *Chebyshev* approximation [32]. As *Boyd* shows, the *Chebyshev* approximation problem can be represented as a linear programming problem.

Parametric models were produced of all experimentally obtained results from the first configuration of the study. The model order was chosen based on practical considerations. The order is set until the maximum level of FIT is reached, while at the same time the model order does not increase significantly. Approximation of all experimental data sets was performed with a 6th-order parametric model, but with different values of the coefficients. The approximation was performed in the frequency range from 100 to 2000 Hz, which was chosen due to the fact that noise can be easily suppressed at higher frequencies. Results are presented for only two pump operating modes: at the minimum rotation frequency 950 min<sup>-1</sup> and minimum pressure load 0 MPa, and at the rotation frequency 1450 min<sup>-1</sup> and maximum pressure load 15 MPa. In the first case, the resulting parametric model is:

$$W_{apr,1}(s) = \frac{191.4s^6 + 4.12 \times 10^6 s^5 + 9.26 \times 10^{10} s^4 + 4.68 \times 10^{13} s^3 + 3.41 \times 10^{17} s^2 + 5.93 \times 10^{19} s + 1.55 \times 10^{23}}{s^6 + 367.6s^5 + 1.87 \times 10^8 s^4 + 5.04 \times 10^{10} s^3 + 2.07 \times 10^{15} s^2 + 1.32 \times 10^{17} s + 2.74 \times 10^{21}}. \quad (15)$$

The comparison between the experimentally measured and approximated frequency responses is presented in Figure 13. The experimental frequency response is depicted with a dashed line in the figure.

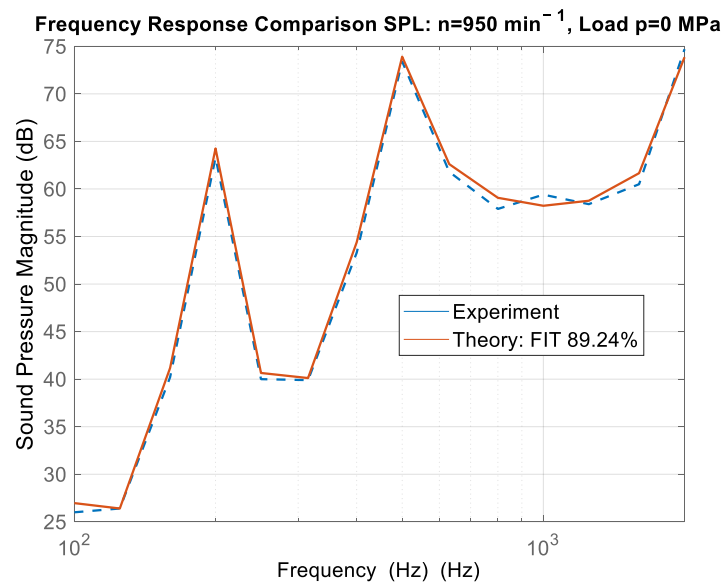


**Figure 13.** Frequency response comparison of  $SPL: n = 950 \text{ min}^{-1}$  & load  $\Delta p = 0 \text{ MPa}$ .

In the second case, the resulting parametric model is:

$$W_{apr,2}(s) = \frac{436.3s^6 + 1.05 \times 10^8 s^5 + 1.03 \times 10^{12} s^4 + 1.25 \times 10^{15} s^3 + 5.75 \times 10^{18} s^2 + 1.41 \times 10^{21} s + 2.89 \times 10^{24}}{s^6 + 1.44 \times 10^4 s^5 + 4.75 \times 10^8 s^4 + 1.24 \times 10^{12} s^3 + 1.10 \times 10^{16} s^2 + 5.02 \times 10^{18} s + 3.39 \times 10^{22}}. \quad (16)$$

The comparison between the experimentally measured and approximated frequency responses is presented in Figure 14.

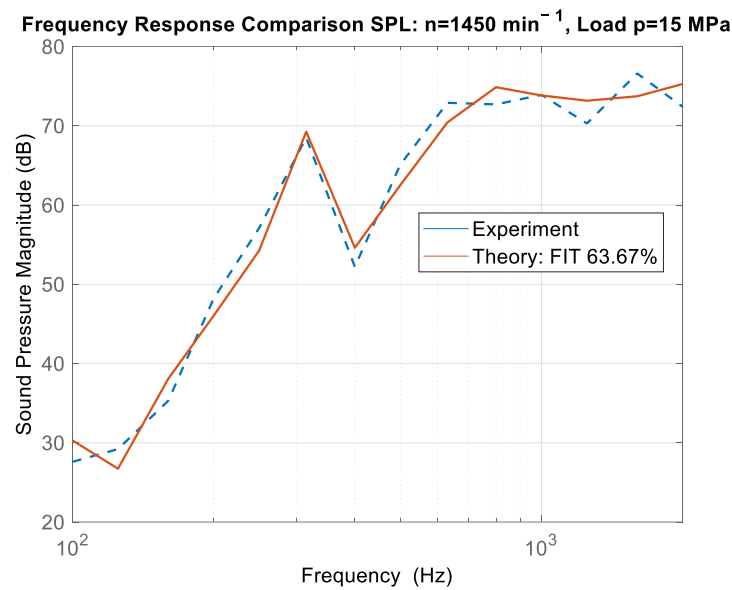


**Figure 14.** Frequency response comparison of  $SPL: n = 1450 \text{ min}^{-1}$  & load  $\Delta p = 15 \text{ MPa}$ .

In finite resolution computer arithmetic, any calculation with real numbers should be examined with respect to rounding errors and numerical stability. Working with large numbers in floating point representation is indeed susceptible to larger relative errors. However, it is well known that such issues can be addressed using various numerical methods, such as arbitrary-precision arithmetic representations, fixed point arithmetic, etc. Even if such measures require additional computational resources, this should not pose a limitation for modern processors.

The analysis of the obtained results was performed by calculating the level of FIT between the experimental and theoretical models [30].

Table 4 shows a numerical comparison between measured and approximated  $SPL$ , expressed as a percentage level of FIT:

$$\text{FIT} = 100 \left( 1 - \frac{\|\hat{S} - S\|_2}{\|S - E(S)\|_2} \right), \% \quad (17)$$

where  $S$  is the measured  $SPL$ ,  $\hat{S}$  is the approximated  $SPL$ , and  $E(\bullet)$  is an averaging operator.

**Table 4.** Level of FIT.

No.	$n_i$	$\Delta p_i$	$\Delta p_{PRV}$	FIT
	$\text{min}^{-1}$	MPa	MPa	%
1		0		89.24
2		5.00		71.60
3	950	7.50	16.00	64.71
4		10.00		81.26
5		12.50		87.18
6		15.00		89.17
1	1450	0	16.00	60.65
2		5.00		68.13
3		7.50		76.05
4		10.00		71.52
5		12.50		67.09
6		15.00		63.67

As can be seen from the results, the level of FIT at the lower rotation frequency is significantly higher than at the higher rotation frequency. This is because at a higher rotation frequency, the sound pressure characteristics have a more pronounced nonlinearity, which is a consequence of the design features of the pump as well as the increase in load. For the purpose of improving the control performance as an active noise reduction measure, a model with this level of FIT with the experimental data is sufficient.

The purpose of the *SPL* approximation model is to establish a linear approximation of the obtained frequency response. The level of fitness is dependent on the selected model order, the number of sample points in the experimental data, and the amount of nonlinearity in the characteristic, and should not be taken as the sole indicator of model performance. It is evident from the presented figures that the parametric model sufficiently reflects the resonance frequencies, average *SPL* and target frequency band. The practical usability of the estimated model will be to guide the design of noise reduction measures at the selected resonance frequencies, which, as can be seen, are well captured in the model.

## 7. Conclusions

The main contribution of this article is to present a data set of experimentally obtained results and an analysis of the sound pressure level caused by a hydraulic power unit based on an external gear pump. The hydraulic power unit uses a common architecture in which the pump is installed inside the tank. In contrast to other similar projects, the experimental study of the *SPL* was carried out under the normal operating conditions in which hydraulic drives for various industrial applications most often operate. The experimental studies were carried out on a laboratory experimental setup, enabling the pump to be tested at different operating modes in terms of rotation frequency and pressure loading. Modern measuring equipment providing various measures, including a class-1 four-channel sound level meter and an acoustic camera, was used. The analysis of the experimental results was carried out using various quantitative indicators assessing the *SPL*: A-weighted *SPL*, average A-weighted *SPL*, maximum *SPL*, minimum *SPL*, and the area of the magnitude frequency response, precisely determined using Riemann's integral formula. The analyses of the results were also confirmed with an acoustic camera with beamforming visualization. The results show which of the indicators provide information for choosing an appropriate rotation frequency and load leading to low *SPL*.

In addition to the main contribution of this study, a method for identification by approximation of experimental data was used that enabled obtaining a parametric model of the magnitude frequency response with an acceptable level of FIT between experimental and theoretical results. The obtained parametric models can be used to reduce the *SPL* by passive or active means (e.g., frequency control of the electric motor). The quantitative analysis can serve as a basis of comparison with results obtained after adding passive (damping ring, etc.) or active means to reduce the *SPL*.

This experimental study can serve as a methodology for the study of other types of machines operating in their normal operating environment, with the aim of selecting operating modes with an optimal *SPL*.

**Author Contributions:** Conceptualization, A.M., K.N. and I.K.; methodology, A.M., K.N. and I.K.; software, K.N.; validation, A.M.; formal analysis, A.M., K.N. and I.K.; investigation, A.M., K.N. and I.K.; resources, A.M.; data curation, A.M.; writing—original draft preparation, A.M., K.N. and I.K.; writing—review and editing, I.K. and A.M.; visualization, A.M.; supervision, I.K.; project administration, K.N.; funding acquisition, I.K. All authors have read and agreed to the published version of the manuscript.

**Funding:** European Regional Development Fund within the Operational Programme “Bulgarian national recovery and resilience plan”, procedure for direct provision of grants “Establishing of a network of research higher education institutions in Bulgaria”, and under Project BG-RRP-2.004-0005, “Improving the research capacity and quality to achieve international recognition and resilience of TU-Sofia (IDEAS)”.

**Data Availability Statement:** Data is available upon request.

**Acknowledgments:** This work has been accomplished with financial support by the European Regional Development Fund within the Operational Programme “Bulgarian national recovery and resilience plan”, procedure for direct provision of grants “Establishing of a network of research higher education institutions in Bulgaria”, and under Project BG-RRP-2.004-0005 “Improving the research capacity and quality to achieve international recognition and resilience of TU-Sofia (IDEAS)”.

**Conflicts of Interest:** The authors declare no conflict of interest.

## References

1. Akers, A.; Gassman, M.; Smith, R. *Hydraulic Power System Analysis*, 1st ed.; Taylor and Francis Group: Abingdon, UK, 2006.
2. ISO 16902-1:2003; Hydraulic Fluid Power—Test Code for the Determination of Sound Power Levels of Pumps Using Sound Intensity Techniques: Engineering Method—Part 1: Pumps. International Organization for Standardization: Geneva, Switzerland, 2003.
3. ISO 3744:2010; Acoustics—Determination of Sound Power Levels and Sound Energy Levels of Noise Sources Using Sound Pressure—Engineering Methods for an Essentially Free Field over a Reflecting Plane. International Organization for Standardization: Geneva, Switzerland, 2003.
4. Jorges, I.H. Noise and Vibration Reduction in Hydraulic Drive Systems. Ph.D. Thesis, TU-Sofia, Sofia, Bulgaria, 1987.
5. Hobbs, J.; Fricke, H.-J. *New Methods of Reducing Noise in External Gear Pumps*; SAE Technical Papers; SAE International: Warrendale, PA, USA, 1980.
6. Fiebig, W.; Wrobel, J. System approach in noise reduction in fluid power units. In Proceedings of the BATH/ASME Symposium on Fluid Power and Motion Control, Bath, UK, 12–14 September 2018.
7. Mucchi, E.; Dalpiaz, G.; Rivola, A. Dynamic behavior of gear pumps: Effect of variations in operational and design parameters. *Meccanica* **2011**, *46*, 1191–1212. [CrossRef]
8. Manring, N.D.; Kasaragadda, S.B. The theoretical flow ripple of an external gear pump. *J. Dyn. Syst. Meas. Control Trans. ASME* **2003**, *125*, 396–404. [CrossRef]
9. Marinaro, G.; Frosina, E.; Senatore, A. A Numerical Analysis of an Innovative Flow Ripple Reduction Method for External Gear Pumps. *Energies* **2021**, *14*, 471. [CrossRef]
10. Mhana, W.; Popov, G. Method for investigation of the pressure variation in the chambers of gear pumps with symmetric and asymmetric tooth profiles used in electrohydraulic drive systems. In Proceedings of the 16th Conference on Electrical Machines, Drives and Power Systems, Varna, Bulgaria, 6–8 June 2019.
11. Li, R.; Liu, Q.; Cheng, Y.; Liu, J.; Sun, Q.; Zhang, Y.; Chi, Y. Analysis of the Influence of Structure and Parameters of Axial Piston Pump on Flow Pulsation. *Processes* **2022**, *10*, 2138. [CrossRef]
12. Fiebig, W. Influence of the inter teeth volumes on the noise generation in external gear pumps. *Arch. Acoust.* **2014**, *39*, 261–266. [CrossRef]
13. Mucchi, E.; Rivola, A.; Dalpiaz, G. Modelling dynamic behaviour and noise generation in gear pumps: Procedure and validation. *Appl. Acoust.* **2014**, *77*, 99–111. [CrossRef]
14. Woo, S.; Opperwall, T.; Vacca, A.; Rigosi, M. Modeling noise sources and propagation in external gear pumps. *Energies* **2017**, *10*, 1068. [CrossRef]
15. Fiebig, W. Noise control of fluid power units. In Proceedings of the 23rd International Congress on Sound and Vibration: From Ancient to Modern Acoustics, Athens, Greece, 10–14 July 2016.
16. Carletti, E.; Pedrielli, F. Sound power levels of hydraulic pumps using sound intensity techniques: Towards more accurate values? In Proceedings of the 12th International Congress on Sound and Vibration, Lisbon, Portugal, 11–14 July 2005.
17. Kojima, E.; Yamazaki, T.; Edge, K. Development of standard testing procedure for experimentally determining inherent source pulsation power generated by hydraulic pump. *Int. J. Fluid Power* **2009**, *10*, 27–35. [CrossRef]
18. ISO 3745:2012; Acoustics—Determination of Sound Power Levels and Sound Energy Levels of Noise Sources Using Sound Pressure—Precision Methods for Anechoic Rooms and Hemi-Anechoic Rooms. International Organization for Standardization: Geneva, Switzerland, 2012.
19. ISO 3747:2010; Acoustics—Determination of Sound Power Levels and Sound Energy Levels of Noise Sources Using Sound Pressure—Engineering/Survey Methods for Use in Situ in a Reverberant Environment. International Organization for Standardization: Geneva, Switzerland, 2010.
20. Svantek. Available online: <https://svantek.com/products/svan-958a-four-channels-sound-vibration-meter/> (accessed on 11 July 2023).
21. ISO 3740:2019; Acoustics—Determination of Sound Power Levels of Noise Sources—Guidelines for the Use of Basic Standards. International Organization for Standardization: Geneva, Switzerland, 2019.
22. ISO 3741:2010; Acoustics—Determination of Sound Power Levels and Sound Energy Levels of Noise Sources Using Sound Pressure—Precision Methods for Reverberation Test Rooms. International Organization for Standardization: Geneva, Switzerland, 2010.
23. CAE Software & Systems. Available online: <https://www.cae-systems.de/en/products/acoustic-camera-sound-source-localization/bionic-m-112.html> (accessed on 11 July 2023).

24. Osiński, P.; Deptuła, A.; Deptuła, A.M. Analysis of the Gear Pump's Acoustic Properties Taking into Account the Classification of Induction Trees. *Energies* **2023**, *16*, 4460. [[CrossRef](#)]
25. Brandt, A. *Noise and Vibration Analysis: Signal Analysis and Experimental Procedures*, 1st ed.; John Wiley and Sons Ltd.: Hoboken, NJ, USA, 2011.
26. McCallum, W.G.; Hughes-Hallett, D.; Flath, D.E.; Gleason, A.M.; Kalaycioglu, S.; Lahme, B.; Lock, P.F.; Lozano, G.I.; Morris, J.; Mumford, D.; et al. *Calculus*, 7th ed.; John Wiley & Sons Inc.: Hoboken, NJ, USA, 2017.
27. Kwong, A.; Edge, K. A method to reduce noise in hydraulic systems by optimizing pipe clamp locations. *Proc. Inst. Mech. Eng. Part I J. Syst. Control Eng.* **1998**, *212*, 267–280. [[CrossRef](#)]
28. Danes, L.; Vacca, A. A frequency domain-based study for fluid-borne noise reduction in hydraulic system with simple passive elements. *Int. J. Hydromechatronics* **2021**, *4*, 203–229. [[CrossRef](#)]
29. Pan, M.; Yuan, C.; Ding, B.; Plummer, A. Novel Integrated Active and Passive Control of Fluid-Borne Noise in Hydraulic Systems. *ASME. J. Dyn. Sys. Meas. Control* **2021**, *143*, 091006. [[CrossRef](#)]
30. Mitov, A.; Krlev, J.; Angelov, I. Design of digital PI regulators from experimental frequency response of electrohydraulic steering system. In Proceedings of the 15th International Conference on Electrical Machines, Drives and Power Systems, Sofia, Bulgaria, 1–3 June 2017.
31. Balas, G.; Chiang, R.; Packard, A.; Safonov, M. *Robust Control Toolbox™ 3 User's Guide*; The MathWorks, Inc.: Natick, MA, USA, 2009.
32. Boyd, S.; Vandenberghe, L. *Convex Optimization*; Cambridge University Press: Cambridge, UK, 2004.

**Disclaimer/Publisher's Note:** The statements, opinions and data contained in all publications are solely those of the individual author(s) and contributor(s) and not of MDPI and/or the editor(s). MDPI and/or the editor(s) disclaim responsibility for any injury to people or property resulting from any ideas, methods, instructions or products referred to in the content.